RSC Advances

ROYAL SOCIETY OF CHEMISTRY

www.rsc.org/advances

Journal Name

ARTICLE

Branched Triphenylamine-cored Compounds: Aggregation Induced Two-photon Absorption

Received 00th January 20xx,
Accepted 00th January 20xx

DOI: 10.1039/x0xx00000x

www.rsc.org/

Xin Zhang[a, ξ], Xiaoping Gan[a, b, ξ], Shun Yao[a], Weiju Zhu[a], Jianhua Yu[a], Zhichao Wu[a], Hongping Zhou[a,*], Yupeng Tian[a], Jieying Wu[a]

Three branched molecules (**T1**-**T3**) were synthesized through simple step to realize or enhance 2PA in aggregates. Spectra data showed that one- and two- branched molecule (**T1** and **T2**) owned the remarkable AIE properties, which came from the formation of *J*-aggregation because of their partial planarization in aggregation state. SEM and DLS illustrated that the ordered aggregation and the small particle size had important influence on fluorescence emission. The open aperture Z-scan experiments showed that **T1** and **T2** possessed excellent 2PA properties under aggregation state. The largest 2PA cross section was 8314 GM for **T2** in aggregates, which was higher about 13-fold than that in pure solution. All the results displayed that the compounds could obtain the outstanding 2PA performance by adjusting their structure rationally or changing state, which could provide reference for preparing the strong 2PA compounds.

Introduction

Organic compounds with excellent two photon absorption (2PA) properties are very important for their real applications such as optoelectronic materials and bio-sensors for metal ions, anions, and neutral small molecules in cells and tissues [1-3], which contributes to more focus on two-photon biological fluorescent probe and commercially application of confocal laser two-photon microscopes [4-6]. In most case, typical π-π stacking interactions often lead to aggregation-caused quenching which seriously limits their applications [7, 8]. Hence, aggregation-induced emission (AIE) or aggregation-induced enhanced emission (AIEE) is proposed by Tang and co-workers to overcome the disadvantage of ACQ [9, 10], which has been attracted the interest of researchers [11-13]. Thus, a few of 2PA materials with AIE or AIEE effects are synthesized, which shows good two-photon bio-imaging ability in cell. For example, Tian' group reported a series of heterocycle replaced 1, 4-bisstyrylbenzene, which functionalized by cyano group in double bond of styrene to produce steric hindrance and then activated AIE performance [14]. These compounds possessed moderate 2PA cross sections (σ) in aggregates in the mixture solution of THF/H_2O, which made them the potential materials for bio-photonic applications. Wu and co-workers reported a series of amino substitutive styrene derivatives that showed good AIE performance in DMSO/H_2O mixture solution and appropriate two-photon excited fluorescence (TPEF)[15]. Consequently, these compounds were applied in two-photon bio-imaging. However, the numbers of the reported 2PA compounds with AIE or AIEE properties are very less, and the structure-activity relationship is not clear. Moreover, their 2PA properties are slightly weak perhaps due to the contradiction between the planarity of 2PA molecules and the twisted conformation of AIE or AIEE molecules. So designing and synthesis of strong 2PA molecule owning AIE or AIEE properties is the key of two-photon bio-imaging and further research is still in need.

It is well known that branched molecules usually possess the synergetic enhancement effect on 2PA properties, while they are not demand for the strict planar structure [16, 17]. Based on the above, we selected triphenylamine as the molecule core to construct branched molecules due to its excellent electron donating ability (D) and variable propeller structure[18]. Meanwhile, we utilized *p*-nitrobenzene as an electron acceptor (A) to form an A-π-D model structure at each branch. The donor and acceptor were connected by carbon-carbon double bond as π-bridge, then we introduced cyano group to the double bond as a multi-functional group due to its bulky volume and abundant π-electron density [19]. Moreover, cyano group was also an outstanding electron withdrawing group, which could adjust the molecule dipole moment and enhance the intramolecular charge transfer (ICT) [20].

[a]*College of Chemistry and Chemical Engineering, Anhui University and Key Laboratory of Functional Inorganic Materials Chemistry of Anhui Province, Hefei 230601, P. R. China.*
[b]*School of Science, Anhui Agricultural University, 230036 Hefei, P. R. China.*
[*]*Corresponding author. Fax: +86-551-63828106, Tel: +86-551-63828150. E-mail address: zhpzhp@263.net*
[ξ]*These authors contributed equally to this work and should be considered co-first authors*

†Electronic Supplementary Information (ESI) available: Figures S2-S8, Tables S1-S3. Crystallographic data have been deposited with the Cambridge Crystallographic Data Centre as supplementary publication no. CCDC: 1428578 (for **T1**), 1437376 (for **T2**).

Herein, linear A-π-D (**T1**), V-shaped ((A-π-)$_2$D) (**T2**) and Y-shaped ((A-π-)$_3$D) (**T3**) molecules (**Scheme 1**) have been synthesized, which used only two-step reaction to give the final products with high yields (over 90%). All compounds are soluble in common organic solvents such as tetrahydrofuran (THF), acetone, ethyl acetate and dimethyl formamide (DMF) but insoluble in water. We systematically researched their one- and two-photon optical properties in pure organic solution and water-organic mixture solution, which showed that **T1** and **T2** both possessed superior AIE performance in ethanol/water and DMF/water solutions, respectively. Moreover, **T1** and **T2** were all provided with excellent 2PA properties under aggregation state, we successfully carried out the two-photon bio-imaging applications based on the favorable biocompatibility.

Results and discussion

Synthesis

The compounds **1**, **2** and **3** were prepared according with the reported method.[21] Then the condensation of 4-Nitrophenylacetonitrile with the respective intermediates **1**, **2** and **3** by the *Knoevenagel* reaction gave the target compounds (**T1**-**T3**). All compounds were characterized by ^{1}H, ^{13}C NMR and mass spectra (shown in ESI, **Fig. S1**)

One-photon absorption and emission properties

The One photon absorption and fluorescence emission spectra of **T1** in five solvents of varying polarities were depicted in Fig. **1**. All the corresponding spectroscopic data were collected in Table S**1**. It could be seen from Fig. 1a that **T1** had two absorption peaks located at ~300 nm and ~430 nm, the former was assigned to the π-π* electronic transition caused by the triphenylamine core[22] whereas the latter was likely ascribed to intramolecular charge transfer between the triphenylamine core and the terminal group. From the Fig. S**2**-**3**, it could be seen that the other two compounds had similar feature in absorption spectra.

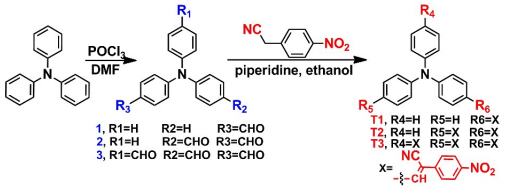

Scheme 1 Preparation of compounds **T1**, **T2**, **T3**

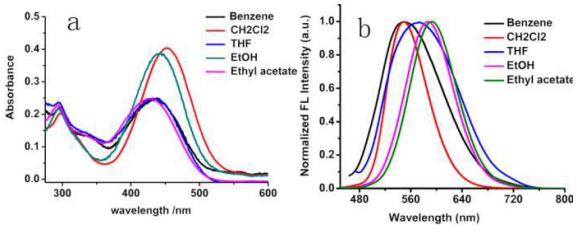

Fig. 1 Linear absorption spectrum (a) and fluorescence spectrum (b) of **T1** in five organic solvents with different polarities at a concentration of 5×10^{-5}mol L^{-1}.

The fluorescence spectrum of **T1** (Fig. **1**b) exhibited one emission peak located from 548 nm to 593 nm in different polarity solvents, which was assigned to the ICT emission.[23] As shown in Table S**1** and Fig **1**b, with increasing the solvent polarity, the fluorescence maxima red shifted from 548 nm to 593 nm with a relevant solvatochromic effect. From the Fig.S**2**-**3**, it could be seen that the other two compounds had similar feature in fluorescence spectra. Large stokes shifts were observed for the three compounds in five solvents due to strong solvent-solute dipole-dipole interactions, which was a manifestation of the large dipole moment and orientational polarizability. An increased dipole-dipole interaction between the solute and solvent generated a lower energy level. Stokes shift were approximately proportional to the orientational polarizability.[24, 25] To discuss the effect of solvents on the fluorescence spectrum, Lippert-Mataga plots [26] for **T1**-**T3** were given in Fig. S**4** and the calculation data were collected in Table S**2**. The Lippert-Mataga equation was as follow:

$$\Delta\nu = \frac{2\Delta f}{4\pi\varepsilon_0 \hbar c a^3}(\mu_e - \mu_g)^2 + b \qquad \text{Eq. (1)}$$

$$\Delta f = \frac{\varepsilon - 1}{2\varepsilon + 1} - \frac{n^2 - 1}{2n^2 + 1} \qquad \text{Eq.(2)}$$

in which $\Delta\nu = \nu_{abs} - \nu_{em}$ stands for Stokes shift, ν_{abs} and ν_{em} are absorption and emission (cm^{-1}), h is the Planck constant, c is the velocity of light in vacuum, a is the Onsager radius and b is a constant. Δf is the orientation polarizability, μ_e and μ_g are the dipole moments of the emissive and ground states, respectively, and ε_0 is the permittivity of the vacuum. $(\mu_e - \mu_g)^2$ is proportional to the slope of the Lippert-Mataga plot.

As shown in Fig. S**4**, the slopes of the fitting line for **T1**-**T3** were as high as 1.7×10^4, 3.1×10^4, and 1.9×10^4, respectively. The large slopes showed large dipole moment changes for these compounds with photoexcitation,[27] which was consistent with the significant solvatochromism effect measured by experiment. However, the slope of **T3** was smaller than that of **T2**, the reason perhaps was that **T3** owned larger Onsager radius due to it has bulky molecule volume.

Aggregation-induced emissions

Considering the three compounds are insoluble in water but soluble in organic solvents, we determine the absorption and emission spectra of the **T1**-**T3** in organic/organic-water mixtures with different water fractions (f_w, the volume percentage of water in organic-water mixtures, that can adjust the solvent polarity subtly). This is revealed by the images in Fig. **2** and Fig. **3**. The absorption spectrum of **T1** has been recorded and shown in Fig. **2**a. We can see that T1 shows two absorption peaks in ethanol which located at ~293 nm and ~441 nm. Meanwhile, the spectra of the mixtures with high f_w values start to show level-off tails in the long wavelength region caused by the Mie scattering effect, which implies the formation of nanoaggregates [28]. Moreover, the two absorption peaks of **T1, T2** both red shift with the increasing of f_w, which is the feature of the *J*- aggregation [29]. As can be seen from the

Fig. **3**a, **T2** in organic-water mixtures also shows similar characteristic of absorption spectrum with **T1**.

The fluorescence spectrum of **T1** in the water-ethanol mixture with different water contents were shown in Fig **2**b, which indicated obvious AIE properties when $f_w \geq 50\%$. The fluorescence intensity primarily decreased with increasing f_w when $f_w \leq 50\%$, then increased with the f_w increasing when $f_w \geq 50\%$. The fluorescence intensity primarily decreased and the emission peak red shifted slightly with increasing f_w when fw≤ 50%, which could be attributed to the twisted intramolecular charge-transfer (TICT) [30, 31], then the fluorescence intensity increased and the emission peak showed remarkable red-shift with the f_w increasing when $f_w \geq 50\%$, which could be ascribed to the formation of a charge-transfer (CT) excited[32, 33] and the formation of *J*- aggregation. The inset depicts the changes of integrated intensity with different water fractions. The fluorescence spectrum of **T2** in the water-DMF mixtures with different water contents were shown in Fig. **3**b. We could see that the fluorescence intensity of **T2** was very weak and showed almost no change as f_w increases from 0% to 30%, while a significant enhancement of fluorescence intensity was observed in the water-DMF mixture when $f_w > 30\%$, accompanying a small red-shift in the spectrum. The highest fluorescence intensity at $f_w = 50\%$ was higher about 17.5-fold than that in the pure DMF solution. Subsequently, with increasing the water fraction, the fluorescence intensity of **T2** was slightly decreased. This was also a typical AIE phenomenon but different with that of **T1**, perhaps because of **T1** itself owned weak fluorescence in ethanol solution while **T2** had no fluorescence emission in pure DMF solution. But, **T3** had no AIE effect in various organic solvents mixed with different proportions of water.

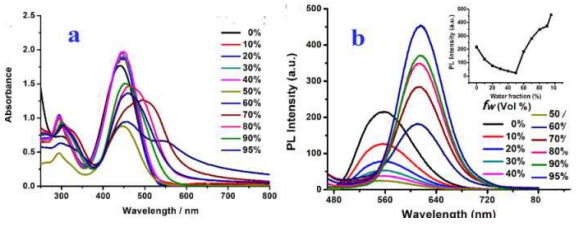

Fig. 2 Absorption (a) and fluorescence (b) spectra of **T1** in water/Ethanol mixtures with f_w at 5.0×10^{-5} M. The inset depicts the changes of fluorescence intensity with different f_w.

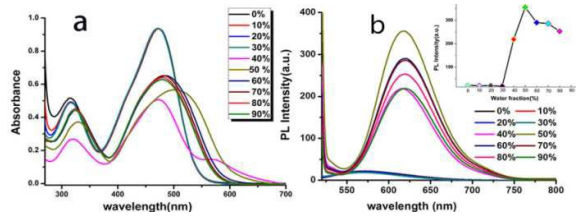

Fig. 3 Absorption (a) and fluorescence (b) spectra of **T2** in water/DMF mixtures with f_w at 5.0×10^{-5}M. The inset depicts the changes of fluorescence intensity with different f_w.

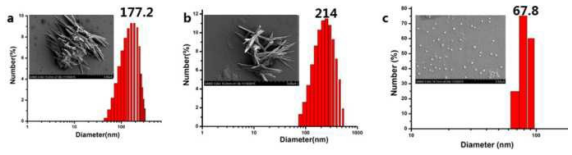

Fig.4 Particle size distribution of **T1** in mixtures with different water fractions: (a) Water/Ethanol (30/70, v/v); (b) Water/Ethanol (50/50, v/v); (c) Water/Ethanol (95/5, v/v). The inset depicts SEM images of **T1** in Ethanol/Water mixtures with the same water fractions as DLS

To gain further insight into the influence of morphology and particle size on AIE properties, we also carried on the scanning electron microscope (SEM) and dynamic light scatting (DLS) for **T1** and **T2** at different water fractions. The SEM images of **T1** were depicted in Fig. **4** (Inset), we could see that the aggregates were formed as a needle-like nanoparticles in the mixture solution when $f_w \geq 30\%$, while a small globular homogeneous nanoparticles formed immediately in the mixture of $f_w = 95\%$, which implied the polarity of the solvent hold important influence on the morphology of the aggregates. The size distribution of **T1** in the mixture solution with different water fractions were conducted by DLS, which presented that the average diameters (d) were 177.2 ($f_w = 30\%$), 214.0 ($f_w = 50\%$) and 67.8 ($f_w = 95\%$) nm (Fig. 4), respectively. The results showed that the orderly aggregates began to form with the addition of water, the particle size increased when $f_w \leq 50\%$ and decreased when $f_w \geq 50\%$, thus led to the maximum fluorescence intensity at $f_w = 95\%$. **T2** also showed the similar size distribution influence on AIE properties in mixture solution of DMF/water at different water fractions. The average diameters (d) of **T2** in different water fractions of DMF/water mixtures were 172.4, 72.5 and 220.4 nm (Fig. S**5**), respectively. The results were agreed with the fluorescence intensity changes at different water fractions. All these results illustrated that the particle size of aggregates had an important effect on their AIE properties.

Mechanisms of emission enhancement

In order to better understand the relationship between the photo physical properties and the molecular structure, single crystals of **T1** and **T2** were obtained through slow evaporation of methanol and acetonitrile solution at room temperature respectively. The crystal structures of the two compounds were shown in Fig. **5** and Fig. S**6**. Their crystallographic data were summarized in Table S**3**.

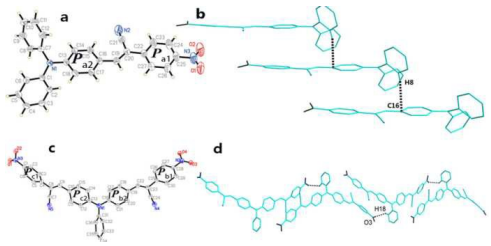

Fig. 5 Crystal structure of **T1** and **T2**, (a) single molecule structure of **T1**, (b) The 1D linear structure of **T1**, (c) single molecule structure of **T2**, (b) The 1D linear structure of **T2**.

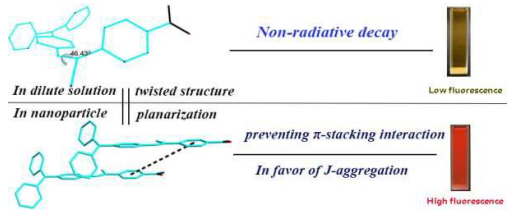

Fig. 6 Proposed mechanism of enhanced emission in nanoparticles of **T1**

As shown in Fig. **5a** and Fig. **5c**, the dihedral angles between the plane of the terminal aromatic ring (P1) and the benzene ring (P2) of the triphenylamine was 1.858° for **T1**, and that of the same position in **T2** was 5.617°, while the dihedral angle of another branch in **T2** was 31.55°. The data indicated that **T1** possessed good planarity in solid state excepting the other two benzene rings while **T2** only held the planarity in one branch. Their stacking structure were exhibited in Fig. **5b** and Fig. **5d**, it could be seen that multiple weak interactions including C8-H8···π (ring: C13, C14, C15, C16, C17, C18) (d= 3.12Å) and C18-H18···O3 (d(H18···O3) =2.588Å, d(C18···O3) =3.246 Å, ∠C18-H18-O3= 128.17º) played an important role on molecular stacking. Benefit by these weak interactions and partial planar structure, **T1** and **T2** both adopt the *J*-aggregation with a head to tail model, which avoided strong π···π stacking and made for fluorescence emission in aggregation state. To confirm these findings, we simulated the single molecule structure of **T1** and **T2** in ethanol by theoretical calculation (Fig. **6** and Fig. **7**) [34]. Fig. **6** showed that **T1** possessed extreme distortion structure with a large dihedral angle (53.53°) between the planes P1 and P2 in dilute ethanol solution. Compared with that in crystal state, we could find that molecule aggregation would result in the increment of the molecule planarity, which enhanced ICT progress and was favourable for the formation of *J*-aggregation. From **Fig**. **7**, we could see that **T2** had the similar feature in dilute solution and in crystal. Thereby, we could imagine that **T3** also had the enhancement of planarity in crystal but not tend to adopt *J*-aggregation due to its steric hindrance caused by three-branched substituent. In one words, aggregation could enhance the molecule planarity and induce to form *J*-aggregation , which could be explained the reason why only **T1** and **T2** owned AIE properties while **T3** did not. On the other hand, **T3** owned three nitro groups which possessed strong electron-withdrawing ability and always quenched fluorescence. As a result, **T3** did not reveal AIE behaviour due to its rather weak fluorescence in aggregated state and in high polar solvent such as DMF and ethanol.

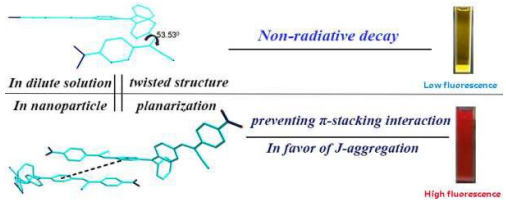

Fig. 7 Proposed mechanism of enhanced emission in nanoparticles of **T2**

Open Z-scan experiment

To investigate the nonlinear optical (NLO) properties of **T1**-**T3**, we conducted the open aperture Z-scan experiments by using a femtosecond laser pulse in pure solution and in aggregates respectively. While for Z-scan measurements, the quartz-glass cell was 1.0 mm thick, and the average laser power was 500 mW. The results were showed in Fig. **8** and Fig. **S7**, the experimental data were illustrated in **Table 1**. The 2PA coefficients (β) for the three compounds were obtained according to Eq. (4):

$$T(Z) = \sum_{m=0}^{\infty} \frac{[-q_0(z)]^m}{(m+1)^{3/2}}, q_0(z) = \frac{\beta I_0 L_{eff}}{(1+z^2/z_0^2)a} \quad \text{Eq.(4)}$$

Where Z_0 is the diffraction length of the beam, I_0 is the intensity of the light at focus, L_{eff} is the effective length of the sample, a is the linear absorption coefficient at the wavelength used. Further, the molecular 2PA cross-section (σ) could be determined through the Z-scan measurement by using the following Eq. (5):

$$\sigma = h\nu\beta \times 10^3 / N_A d \quad \text{Eq.(5)}$$

Where h is Planck's constant, ν is the frequency of input intensity, N_A is the Avogadro constant, and d is the concentration of the sample. From Table **1**, we could see that all the three compounds possessed the enhanced 2PA properties in aggregates compared with that in pure solution. It was interesting that the 2PA property of **T1** changed obviously from pure solution to aggregates, which showed distinct aggregation-induced two photon absorption. Moreover, **T2** displayed remarkable enhancement of 2PA cross section that changed from 947 GM in pure solution to 8314 GM in aggregates [35]. All these results illustrated that aggregation progress could be applied in designing of 2PA materials especially for the aggregation caused by branched compounds.

Cytotoxicity tests

Cytotoxicity was a potential side effect of compounds that must be controlled when dealing with living cells or tissues. Considering their application in cell imaging, the 3-(4, 5 - dimethylthiazol - 2 - yl) - 2, 5 - diphenyltetrazolium bromide (MTT) assay [36] was performed to ascertain the cytotoxic effect of **T1-T3** against HepG2 cells over a period of 24 h. Fig. **9** showed the cell viability for HepG2 cells treated with **T1-T3** at different concentrations. The results clearly indicated that no

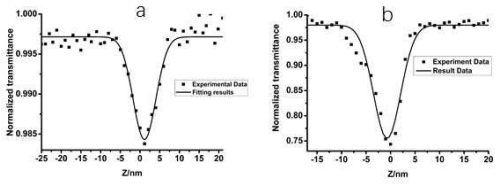

Fig. 8 The open aperture Z-scan plot for **T2** in aggregates (a) and in pure solution (b)

Table 1 2PA cross sections for **T1-T3** in different states

Compounds	T1	T2	T3
Wavelength(nm)	780	820	860
σ(GM) in pure solution	N/A	947	756
σ(GM) in aggregates	4986	8314	925

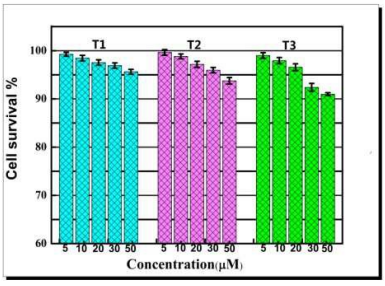

Fig. 9 Cytotoxicity data obtained from the MTT assay in different concentrations for 24 h

obvious cell viability decreased, even when the concentrations of the compounds reached up to 50 μM, the cell viability was still greater than 90%. The low cytotoxicity of the target compounds over a period of at least 24 h indicated it was suitable for cellular imaging applications. This is an important factor in further potential live cell imaging applications due to their relatively low cytotoxicity.

One- and two-photon fluorescence microscopy cell imaging

To demonstrate the applicability of **T1-T3** in cellular imaging, the bio-imaging experiments were carried out by confocal laser scanning microscopy using HepG2 (human liver cancer cells) as an example, the tested compounds were dissolved in DMSO and then serially diluted in complete culture medium. We initially carried out time-dependent two-photon fluorescence. As a consequence, the three compounds all showed good photo-stability to laser power as the time went by, only ~15% signal deduction was observed (Fig. S**8**). The results indicated that these compounds were very suitable for using in biological applications.

Then we carried out bio-imaging studies in living HepG2 cells stained with **T1-T3** by both one- and two-photon microscopy. The excitation wavelength was fixed at their maximum absorption wavelength in one-photon microscopy imaging. As shown in Fig. **10**a, bright green fluorescence with similar intensity from the cells indicated that **T1-T3** could be effectively internalized by HepG2 cells. The three compounds all went through the membrane and localized uniformly in the

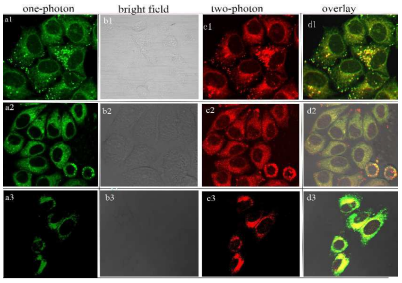

Fig. 10 (a1- a3) one-photon images of HepG2 cells incubated with **T1-T3**, (b1-b3) bright field images of HepG2 cells with **T1-T3**, (c1-c3) two-photon images of HepG2 cells incubated with **T1-T3**, (d1-d3) merged images of HepG2 cells incubated with **T1-T3**.

cytoplasm, which suggested that only the cell cytoplasm could be labelled by these compounds.

Two-photon fluorescence microscopy provides key advantages over one-photon fluorescence imaging, namely, increased penetration depth, lower tissue auto-fluorescence and self-absorption, and reduced photo damage and photo bleaching[37]. As shown in Fig. 10c, the two photon microscopy images of HepG2 cells showed bright red fluorescence in cytoplasm, but **T2** owned better two-photon fluorescence imaging ability than that of **T1** and **T3**, which could be seen from the Fig.10d, the merged pictures of one- and two-photon microscopy. The photograph in Fig. **10**d of **T2** stained HepG2 cells showed obvious strong yellow fluorescence in cytoplasm, while there was only partly yellow fluorescence in cytoplasm stained by **T1** and **T3**. The result could be explained by the reason that the intracellular environment was water soluble which led to aggregation of organic compounds easily, while **T1** and **T2** possessed good AIE performance but **T3** had no AIE effect, hence **T2** demonstrated excellent two photon bio-imaging performance.

Conclusion

In this work, we reported a series of branched polar molecules to realize 2PA and improve 2PA in aggregate through forming *J*-aggregation caused by the branched structure which possessed partial planarity in one branch at solid state and fixed steric hindrance in the other two branches. Their excellent 2PA and AIE properties made us successfully applied them in two photon bio-imaging. The structure-property relationship was summarized clearly and all the results displayed that the branched compounds also possessed outstanding 2PA performance in aggregates by adjusting their structure rationally and changing state, which could provide reference for designing 2PA compounds.

Experimental section

Materials and measurements

Chemicals were purchased and used as received. Every solvent was purified as conventional methods beforehand. ^{1}H, ^{13}C NMR were recorded on 400 MHz and 100 MHz NMR instruments using DMSO as solvent. Chemical shifts were reported in parts per million (ppm) relative to internal TMS (0

ppm) and coupling constants in Hz. Splitting patterns were described as singlet (s), doublet (d), triplet (t), quartet (q) or multiplet (m). The mass spectra were obtained on a Bruker Autoflex III smart beam mass spectrometer. The X-ray diffraction measurements were performed on a CCD area detector using graphite monochromated MoKa radiation (λ = 0.71069 (Å) at 298 (2) K. The non-hydrogen atoms were refined anisotropically and hydrogen atoms were introduced geometrically. Calculations were performed with SHELXTL-97 program package. Dynamic light scattering (DLS) measurements were conducted on a Malvern Zetasizer Nano ZS90 size analyzer. The one-photon absorption (OPA) spectra were recorded on the UV-3600 spectrophotometer. The one-photon emission fluorescence (OPEF) spectra measurements were performed using a Hitachi F-7000 fluorescence spectrophotometer. The quartz cuvettes used were of 1 cm path length. The slit pass width of emission spectra: 10 nm, Voltage: 500 V. 2PA cross sections (σ) of the samples were obtained by Open Aperture Z-scan method and Ti: sapphire system (680-1080 nm, 80 MHz, 140 fs) as the light source.

Synthesis

Synthesis of the intermediate 1-3. The compounds **1**, **2** and **3** were prepared according with the reported method.

Synthesis of compounds T1-3. Compound **1** (273 mg, 1 mmol) and 4-Nitrophenylacetonitrile (194 mg, 1.2 mmol) were dissolved in 30 mL of absolute ethyl alcohol, then piperidine was added in catalytic amount (1 mL) and the reaction mixture was refluxed at 80 ºC for 2 h. After the reaction finished, the solvent was removed via vacuum filter and dried to give a red powder (379.44 mg, yield: 91%). **T1**: ^{1}H NMR (DMSO-d_6, 400 MHz, ppm) δ: 6.95 (d, J = 8.4 Hz, 2H), 7.17-7.23 (m, 6H), 7.42 (t, 4H), 7.92 (d, J = 8.4 Hz, 2H), 7.98 (d, J = 8.4 Hz, 2H), 8.15 (s, 1H), 8.32 (d, J = 8.4 Hz, 2H). ^{13}C NMR (DMSO-d_6, 100 MHz, ppm) δ: 103.70, 118.01, 119.21, 124.29, 125.10, 125.22, 125.96, 126.30, 129.94, 131.52, 140.84, 145.56, 145.69, 146.75, 150.37. MS (m/z): $[M+H]^+$, calcd: 418.1477; found, 418.1538.

T2 and **T3** were obtained as red powders both over 90% yield by following the similar procedure of **T1**. **T2**: ^{1}H NMR (DMSO-d_6, 400 MHz, ppm) δ: 8.33-8.31 (d, J = 8.0 Hz, 4H), 8.21 (s, 2H), 8.01-7.98 (d, J =8.4, 8H), 7.49-7.45 (t, J = 7.6 Hz, 2H), 7.32-7.29 (t, J = 7.4 Hz, 1H), 7.23-7.21 (d, J =7.6, 2H), 7.18-7.16 (d, J = 8.0 Hz, 4H). ^{13}C NMR (DMSO-d_6, 100 MHz, ppm) δ: 148.88, 146.91, 145.27, 145.09, 140.47, 131.51, 130.24, 127.54, 126.69, 126.50, 126.01, 124.29, 122.56, 117.71, 105.32. MS (m/z): $[MH]^+$, calcd: 590.1750; found 590.1750. **T3**: ^{1}H NMR (DMSO-d_6, 400 MHz, ppm) δ: 8.36-8.34(d, J = 8.4 Hz, 6H), 8.29(s, 3H), 8.08-8.02(q, J =7.4Hz, 12H), 7.32-7.30(d, J =8.4 Hz, 6H). ^{13}C NMR (DMSO-d_6, 100 MHz, ppm) δ: 106.35, 117.55, 124.33, 124.78, 126.75, 128.93, 131.64, 140.35, 145.22 147.11, 148.17. MS (m/z): $[M+H]^+$, calcd: 762.2023; found 762.9845.

Cytotoxicity assays in cells

To ascertain the cytotoxic effect of the three compounds, the MTT assay was performed. HepG2 cells were trypsinized and plated to ~70% confluence in 96-well plates 24 h before treatment. Prior to the compounds' treatment, the dulbecco's modified eagle medium (DMEM) was removed and replaced with fresh DMEM, and aliquots of the compound stock solutions (1 mM DMSO) were added to obtain final concentrations of 5, 10, 20, 30 and 50 mM. The treated cells were incubated for 24 h at 37 ℃ and under 5% CO_2. Subsequently, the cells were treated with 5 mg / mL MTT (40 μL/well) and incubated for an additional 4 h (37 ℃, 5% CO_2). Then, DMEM was removed, the formazan crystals were dissolved in DMSO (150 μL/well), and the absorbance at 570 nm was recorded. The cell viability (%) was calculated according to the Eq. (5):

$$Cell\ viability(\%) = \frac{OD_{570}(sample)}{OD_{570}(control)} \times 100 \quad Eq.(5)$$

Where OD_{570} (sample) represents the optical density of the wells treated with various concentration of the compounds and OD_{570} (control) represents that of the wells treated with DMEM + 10% fetal calf serum (FCS). Three independent trials were conducted, and the averages and standard deviations are reported. The reported percent cell survival values are relative to untreated control cells.

Acknowledgments

This work was supported by The National Natural Science Fou ndation of China (21271003, 21271004, 51432001 and 514720 02), Science and Technology Plan of Anhui Province (1604b06 02016), the Ministry of Education of the People's Republic of China, Higher Education Revitalization Plan Talent Project of Anhui Province (2013).

Notes and References

1 J. L. Geng, C. C. Goh, N. D. Tomczak, J. Liu, R. R. Liu, L. Ma, L. G. Ng, G.G. Gurzadyan and B. Liu, *Chem. Mater.,* 2014, 26, 1874-1880.
2 X.Liu, Y. M. Sun, Y. H. Zhang, F. Miao, G. C. Wang, H. S. Zhao, X. Q. Yu, H. Liu and W. Y. Wong, *Org. Biomol. Chem.,* 2011, 9, 3615-3618.
3 A. R. Morales, A. Frazer, A. W. Woodward, H. Y. A. White, A. Fonari and K. D. Belfield, *J Org. Chem.,* 2013, 78,1014-1025.
4 W. Huang, F. S. Tang, B. Li, J. H. Su and H. Tian, *J. Mater.Chem. C.,* 2014, 2, 1141-1148.
5 L. Kong, Y. P. Tian, Q. Chen, Q. Zhang, H. Wang, D. Tan, et al. *J. Mater. Chem. C,* 2015, 3, 570-581.
6 T. Jiang, Y. Qu, B. Li, Y. Gao and J. Hua, *RSC Adv.,* 2015, 5, 1500-1506.
7 D. D. Li, Y. P. Zhang, Z. Y. Fan, J. Chen, J. H. Yu. *Chem. Sci.*, 2015, **6**, 6097-6101.
8 D. Zhang, Y. Gao, J. Dong, Q. Sun, W. Liu, S. Xue and W. Yang, *Dyes Pigments.,* 2015, 113, 307-311.
9 X. Zhang, X. Zhang, L. Tao, Z. Chi, J. Xu and Y. Wei, J. Mater. Chem. B, 2014, 2, 4398–4414.
10 Y. Hong, J. W. Y. Lam and B. Z. Tang, *Chem. Soc. Rev.,* 2011, 40, 5361-5388.
11 C. W. T. Leung, Y. Hong, S. Chen, E. Zhao, J. W. Y. Lam and B. Z. Tang, *J. Am. Chem. Soc.,* 2013, **135**, 62-65.
12 A. Qin, J. W. Y. Lam and B. Z. Tang, *Prog. Polym. Sci.,* 2012, 37, 182-209.

13 Y. Z. Xie, G. G. Shan, P. Li, Z. Y. Zhou and Z. M. Su, *Dyes Pigments.,* 2013, 96, 467-474.
14 B. Wang, Y. Wang, J. Hua, Y. Jiang, J. Huang, S. Qian and H., Tian, *Chem-Eur. J.,* 2011, **17**, 2647-2655.
15 Y. Liu, M. Kong, Q. Zhang, Z. Zhang, H. Zhou, S. Zhang and Y. Tian, *J. Mater.Chem. B.,* 2014, 2, 5430-5440.
16 M. Rumi, J. E. Ehrlich, A. A. Heikal, J. W. Perry, S. Barlow, T. C. Parker C. Parker, H. Rockel, S. Thayumanavan, S. R. Marder, D. Beljonne and J. L. Brédas, *J. Am. Chem. Soc.,* 2000, 122, 9500-9510.
17 Y. Gao, Y. Qu, T. Jiang, H. Zhang, N. He, B. Li and J. Hua, *J. Mater.Chem. C.,* 2014, 2, 6353-6361.
18 X. Gan, Y. Wang, X. Ge, W. Li, X. Zhang, W. Zhu and Y. Tian, *Dyes Pigments.,* 2015, 120, 65-73.
19 B. An, J. Gierschner, S. Park. *Acc. Chem. Res.,*2012, **45**, 544
20 G. Zhang, M. Aldred, W. Gong, C. Li, M. Zhu. Chem Commun., 2012,**48**:7711.
21 M. Thomas, G. Said, M. Meziane, B. Mireille. M. Olivier. *Synthesis.,* 2015, **11**:1771-1774.
22 D. D. Li, X. S. Sun, M. M. Wang, H. Yu, H. P. Zhou, J. Y. Wu. *Sensors and Actuators B.,* 2015, **220**, 1006–1016.
23 H. Detert, V. Schmitt. *J Phys Org Chem.,* 2006, **19**:603-607.
24 F. Jin, D. Xu, H. Zhu, Y. Yan, J. Zheng, J. Zhang, et al. *Dyes Pigments.,* 2014, **109**:42-53.
25 Z. Grabowski, K. Rotkiewicz, W. Rettig. *Chem Rev.,* 2003, **103**:3899-4032.
26 X. P. Ge, X. P. Gan, Y. Shun, K. Wang, W. J. Zhu, J. H. Yu. *J. Mater. Chem. B.,* 2016, **4**, 2785--2793
27 L. Wang, Z. Zheng, J. Yu, J. Zheng, M. Fang, J. Wu, et al. J Mater Chem C., 2013, **1**:6952-6959.
28 R. Araya, V. Andino-Pavlovsky, R. Yuste, R. Etchenique. ACS Chem Neurosci., 2013, **4**:1163-1167.
29 Q. Q. Zhao, J. G. Liu, H. Y. Wang, M. G. Li, K. Zhou, H. Yang, et al. *J. Mater. Chem. C,* 2015, 3, 8183-8192.
30 M. Chen, L. Z. Li, H. Nie, Y. Shi, J. Mei, J. Wang, et al. *Chem. Commun.,* 2015, **51**, 10710-10713.
31 M. Chen, H. Nie, B. Song, L. Z. Li, A. J. Qin, B. Z. Tang. *J. Mater. Chem. C.,* 2016, **4**, 2901-2908.
32 Y.Zhang, K.Wang, G.Zhuang, Z. Xie, C. Zhang, F. Cao, et al. Chem. Eur. J. 2015, 21, 2474 – 2479.
33 a) X. Du, J. Qi, Z. Zhang, D. Ma, Z. Y. Wang, *Chem. Mater.*, 2012, **24**, 2178 – 2185; b) Z. R. Grabowski, K. Rotkiewicz, W. Rettig, *Chem. Rev.,* 2003, **103**, 3899 – 4032; c) Z. H. Guo, T. Lei, Z. X. Jin, J. Y. Wang, J. Pei, *Org. Lett.,* 2013, **15**, 3530 – 3533; d) X. Y. Shen, Y. J. Wang, E. Zhao, W. Z. Yuan, Y. Liu, P. Lu, A. J. Qin, Y. G. Ma, J. Z. Sun, B. Z. Tang, *J. Phys. Chem. C.,* 2013, **117**, 7334 – 7347.
34 Y. Jiang, Y. Wang, J. Hua, J. Tang, B. Li, S. Qian, et al. Chem Commun., 2010, **46**:4689-4691.
35 Y. Gao, Y. Qu, T. Jiang, H. Zhang, N. He, B. Li, et al. *J Mater Chem C.,* 2014, **2**:6353-6361
36 Z. Zheng, Q. Zhang, Z. Yu, M. Yang, H. Zhou, J. Wu, et al. J Mater Chem C., 2013, **1**:822-1830.
37 D. Xu, Z. Yu, M. Yang, Z. Zheng, L. Zhu, X. Ye, et al. *Dyes Pigments.,* 2014, **100**:142-149.

Three branched dipole molecules (**T1**-**T3**) were designed and synthesized. Spectra data showed that one- and two- branched molecule (**T1** and **T2**) owned remarkable AIE properties, which came from the formation of *J*-aggregation because of their partial planarization in aggregation state. The open aperture Z-scan experiments showed that **T1** and **T2** possessed excellent 2PA properties under aggregation state and the largest 2PA cross section was 8314 GM for **T2** in aggregates, which was higher about 13-fold than that in pure DMF solution.